Eur. Phys. J. Plus (2022) 137:1276
https://doi.org/10.1140/epjp/s13360-022-03489-7

THE EUROPEAN PHYSICAL JOURNAL PLUS

Regular Article

Numerical investigation of CPU cooling with micro-pin–fin heat sink in different shapes

Ferhat Koca[1,a], **T. Burak Güder**[2,b]

[1] Department of Mechatronic Engineering, Faculty of Technology, Sivas Cumhuriyet University, Sivas, Turkey
[2] Institute of Science, Energy Science and Technology Engineering, Sivas Cumhuriyet University, Sivas, Turkey

Received: 7 September 2022 / Accepted: 12 November 2022

Abstract The fact that today's computers transmit too much information at effective speeds causes high heat concentrations. These heat concentrations increase the temperature of the computer processor and cause it to deteriorate its consistency and reduce its performance. In the scope of the study offered, the heat transfer performance of the circular, square and triangular fins placed on the heat source of the models created were examined in the range $500 \leq \mathrm{Re} \leq 10{,}000$. A constant heat flux of 2000 W/m^2 was applied to the bottom surface of the heat source. The inlet temperature of the air used as an operating fluid was 300 K, and the atmospheric pressure was accepted as an outlet boundary condition. Analyses were made with Ansys Fluent program. In the study, 4 different models were used as finless, circular finned, square finned and triangular finned models. Nusselt numbers, temperature distributions, pressure drops, friction factor and thermal performance factor values were examined and analyzed for 7 different Reynolds number. As a result, it was revealed that the best work in terms of heat transfer in the examined models was between Re = 5000 and Re = 6500. At Re = 5000, the PEC number, which is the thermal performance factor of the circular finned model, was 17.96% and 18.30% higher, respectively, than the PEC numbers of the square and triangular finned models.

List of Symbols

A	Area
c_p	Specific heat capacity (kJ/kg K)
D_h	Hydraulic diameter (mm)
f	Friction coefficient factor
H	Height of the heat sink (mm)
L	Length of the heat sink (mm)
h	Coefficient of heat transfer (W/m^2 K)
k	Heat conductivity (W/m K)
Nu	Nusselt number
P	Pressure (Pa)
q"	Heat flux (W/m^2)
Re	Reynolds number
T	Temperature (K, °C)
U_m	Mean velocity, (m/s)
w	Heat sink width (mm)
x, y, z	Cartesian coordinates
ρ	Density of fluid
μ	Dynamic viscosity (Pa s)
avg	Average value

[a] e-mail: ferhatkoca@cumhuriyet.edu.tr (corresponding author)
[b] e-mail: t.berk26@hotmail.com

Published online: 23 November 2022

1 Introduction

Computers have become more widespread in all areas of human life with the rapid development of information technologies. The ability of today's computers to transfer a lot of information at high speeds causes high heat concentrations. It is also inevitable that the temperature of the processor increases in this way. In addition, the shrinkage and complex designs in the computer structure cause hot spots on the motherboard and processor. This affects the stability and performance of the processor and also reduces the cooling efficiency.

Heat generated in electronic circuits is a big problem. High heat causes the performance of electronic devices used in almost every field such as defense industry, education and health to decrease and even to become unusable. Problems that may occur in computers using these electronic systems will not only cause disruption of services, but also negatively affect human life. Therefore, researches are carried out to increase the performance and life of electronic devices. It is essential to cool the processor so that the information technology equipment has the appropriate temperature and reliable operating conditions, but it is a very difficult problem to achieve the desired or targeted heat transfer rate, especially in such devices where cooling is a serious problem. For this reason, channels covered with fins from the inside or outside have been developed in order to increase the amount of heat transfer. Channels with external fins can occasionally cause problems in terms of volume and placement. On the other hand, internal fin channels, which is a very effective method, are used in many heat exchangers [1]. Systematic and regular studies on the subject are carried out by researchers all over the world [2–6]. One of the most effective cooling methods in this regard is the use of micro-fins on the heated surface [7–10].

Since the micro-fin surfaces increase the surface area of the area to be cooled, the surface area that the fluid contacts with also increases. In addition, micro-fins provide turbulence to the flow, which is one of the necessary parameters to improve heat transfer; thus an improvement in convection heat transfer is achieved. In a micro-pin–fin heat sink, the improvement of heat transfer is managed together with the excitation of fluid mixing, interruption of the thermal boundary layer, and an enlarged effective surface area for optimum heat exchange [11].

A wide range of experimental and numerical studies aim to explore the hydrothermal aspects of the needle-finned heat sink, which depend on several factors including pin–fin morphology, arrangement, porosity and tip spacing, interfin spacing, flow rate and dispersion [11–13]. A limited number of studies have combined thermal performance optimization of a micro-pin–fin heat sink using nanofluid coolers. The author has previously examined the effect of microchannel outlet cross section location variation on thermal performance [14].

Abbasi et al. mounted a triangular prism inside the pipe to examine the forced convection heat transfer in a 2D horizontal channel with the SIMPLER algorithm and the finite element method. They found that the presence of a triangular prism for $Re > 45$ in periodic flow increases the heat transfer strongly, while the effect of the triangular prism on heat transfer is weak in the case of $Re < 45$ in symmetrical flow. They observed an 85% increase in Nu number at $Re = 250$ value in the study, where the Re number range was selected as 20–250 [15]. Abraham et al. investigated the heat transfers in laminar, turbulent and transition regimes under constant heat flux and constant wall temperatures using liquid in pipe flow with a constant inlet turbulent density of 5%. They found that the heat transfer coefficients are equal in the fully developed turbulent flow, and the heat transfer coefficient of the studies performed with the constant heat flux in the transition regime is 25% higher [16]. Abuşka et al. investigated the effect of air blowing direction on thermal performance with a fan using thermal imaging method. They designed a conical heat sink with a truncated end for their work. The performances of the fins were tested by changing their direction (an option for energy saving) in blowing and pulling. The heat sink was tested at the same fan power for pushing and pulling conditions for 25, 50, 75 and 100 W resistance heater power. 39 fins with a base diameter of 6 mm, a ceiling diameter of 1 mm and a blade length of 10 mm were used. They observed that conical surface heat sinks give better thermal performance when the fan was in the pushing position [17]. Ambreen and Kim investigated the flow and heat transfer characteristics around the square cylinder with corner modifications. In the study, sharp, round, cut and recessed profiles were studied and corner modifications were used to create vortices. They worked in the laminar flow regime by choosing the Reynolds range as 55–200. As the Reynolds number increases, they observed an increase in the eddy formation while the friction factor decreased, and concluded that this phenomenon also increased the heat transfer. They concluded that the Nusselt number increase was 7% higher in the recessed cylinder, 16% in the rounded-corner cylinder, and 20% higher in the cut-corner cylinder compared to the sharp-edged cylinder at $Re = 200$ [18]. Arya et al. presented a study in which they examined heat transfer and fluid flow values using a mixture of magnesium oxide (MgO) and ethylene glycol in a heat exchanger. As a result of the research, they developed the heat transfer coefficient with the changes in flow rate and mass concentrations. They found that as the Reynolds number increases, there is an increase in the heat transfer and a large increase in the heat transfer coefficient in the turbulent regime [19]. Acharya used I-Figure rectangular fins of different lengths and performed hydrothermal analysis of Ag-MgO-Water Hybrid nanofluid flows, which were magnetically affected by natural convective laminar. He generated various velocities, isotherms, streamlines and Nusselt number plots to disclose the impact of different fins' lengths on the thermal control and flow behavior. He indicated that numerically higher heat transmission is realized for Rayleigh numbers, nanoparticle concentrations, and for $AR = 1.1$. [20]. Acharya and Chamkhab examined the Al2O3-Water Nanofluidic movement in a hexagonal space partially heated under the magnetic effect. They also placed fins in hexagonal cavity. In order to address parametric consequences, researchers have drawn various flow lines, speed, isotherm and Nusselt number variations and showed the relationship between Ha, Ra and Nu numbers.

They reported that increasing fins' height fosters heat transport, and the central position of fins' are the most optimized and effective way to amplify heat transport compared to other formations of fins [21].

As we know from daily life and often emphasized in the literature, cooling electronic devices is extremely important for device life and effective usability. At this point, the use of fins on the desired surfaces of heat transfer provides a significant advantage. As Acharya [22] stated, fins are introduced in numerous engineering applications related to heat exchangers, gas turbines, electric transformers, semiconductor devices, air-cooled engines, automobile radiators, hydrogen fuel cells, etc. This research, which is affected by the above mentioned literature and important applications of the fins in different geometric configurations, aimed to improve the heat transfer by using a micro-fin heat sink in the flow area for the processor. Investigations were made for the different Reynolds numbers of the fluid, finless, the circular fin, square fin and triangular fin geometries of aluminum microfins. Thus, examining the heat transfer in models with different geometries will contribute to the improvement of cooling performance in electronic devices. At the end of the research, the following questions are asked to clarify:

- How do geometries affect streamlines and temperature contours?
- How does the increase in Re number, which is one of the most important dimensional number in fluid dynamics, affect the hydro-thermal performance?
- What are the implications of different fin geometries on Nusselt numbers, skin friction and PEC?

2 Material and method

This study deals with the transfer of heat generated in a computer processor by forced convection. Therefore the investigation is not for the whole computer chassis system, but a smaller domain (CPU) in order to simplify the work. The 13 mm × 11 mm cross-sectional area of CPU was taken which is commercially available AMD CPU. For simplicity, the mother board, chipset card are modeled as zero thickness with heat generated uniformly. The models used in the study were obtained from the main geometry adopted by Bhattacharyya et al. [23] available in the literature.

The basic and variable parameters of the model geometries are shown in Fig. 1, and their values are given in Table 1. It was assumed that the upper surfaces and outer walls of the microchannel with size L1 × W are adiabatic. The base of the heat sink (L1 × W2) under the pin fins was exposed to a constant heat flux of 2 kW/m^2. The air used as the refrigerant directed by the inlet section flows over the pin fins before exiting the outlet surface section. The flow was investigated in the range of Re number 500 < Re < 10,000, depending on the hydraulic diameter with the pin [24, 25]. The thermal performance was investigated for the finless and 3 different fin models shown in Fig. 1, as well as the different Re number. These models were named as circular finned, square finned and triangular finned.

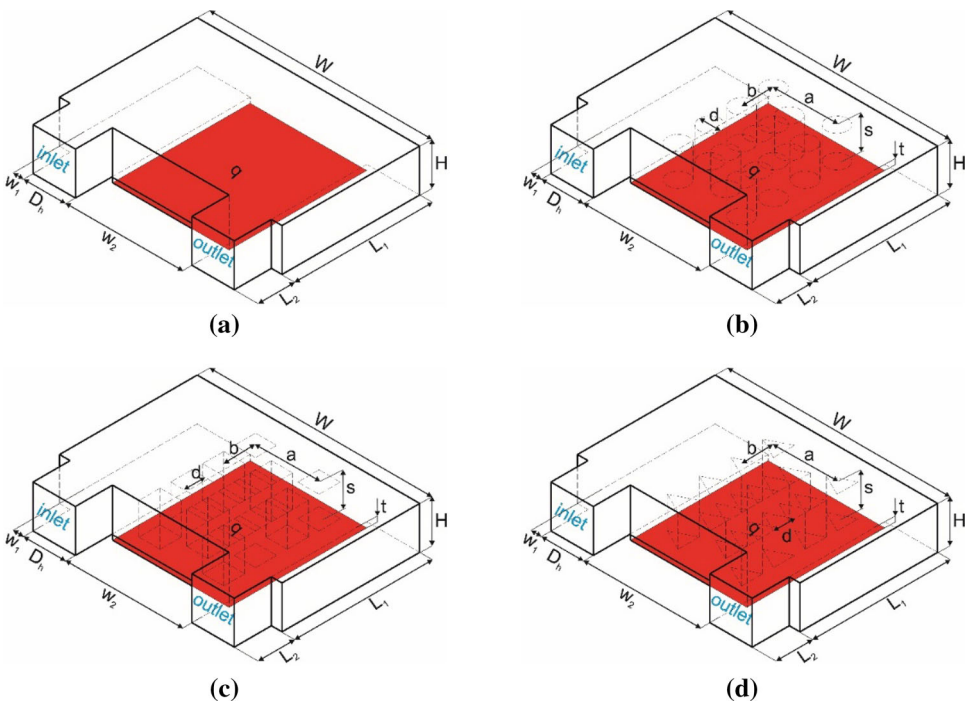

Fig. 1 Dimensional views of models with microchannel **a** finless, **b** circular finned, **c** square finned and **d** triangular finned

Table 1 Micro-pin–fin heat sink parameters and dimensions

Parameter	W	W_1	W_2	L_1	L_2	D_h	H	d	d_1	d_2	t	S	a	b
Dimension (mm)	21	1	11	13	3.5	4	4	2	1.4	1.7	3	3	6	3

3 Mathematical expressions

As can be seen from the geometric models shown in Fig. 1, analyses are performed by using both the fluid zone and the solid zone together in the solution of the micro-pin–fin heat sink.

Continuity, momentum and energy conservation equations were set as given in Eqs. 1,2 and 3 [26]:

$$\nabla.(\rho u) = 0 \tag{1}$$

$$u.\nabla(\rho u) = -\nabla p + \mu\nabla^2 u \tag{2}$$

$$u.\nabla T = k.\nabla^2 T/\rho c_p \tag{3}$$

Air was used as the working fluid in all models and conditions. In the expressions given in the equations: $\rho = 1{,}225$ kg/m^3, $k =$ 0,0242 W/(m K), $cp = 1006{,}43$ J/(kg K), $\mu = 1{,}7894 \times 10{-}5$ kg/(ms). Here; ρ, k, cp and μ stand for density, thermal conductivity, specific heat and viscosity, respectively.

In order to define turbulent flow in forced convection heat transfer analysis, the standard k-ω turbulence model, which is one of the analysis models frequently used in the literature, was used. From the RANS modelling point of view, the $k-\omega$ model offers several advantages relative to the $k-\varepsilon$ model. The most prominent one is that the equations can be integrated without additional terms through the viscous sublayer. Furthermore, the $k-\omega$ model is typically better in predicting adverse pressure gradient boundary layer flows and separation [27]. Kinematic eddy viscosity, turbulence kinetic energy and specific dissipation rate are as follows [28]:

$$v_T = \frac{k}{\omega} \tag{4}$$

$$\frac{\partial k}{\partial t} + U_j\frac{\partial k}{\partial x_j} = \tau_{ij}\frac{\partial U_i}{\partial x_j} - \beta^* k\omega + \frac{\partial}{\partial x_j}\left[(v + \sigma^* v_T)\frac{\partial k}{\partial x_j}\right] \tag{5}$$

$$\frac{\partial \omega}{\partial t} + U_j\frac{\partial \omega}{\partial x_j} = \alpha\frac{\omega}{k}\tau_{ij}\frac{\partial U_i}{\partial x_j} - \beta\omega^2 + \frac{\partial}{\partial x_j}\left[(v + \sigma v_T)\frac{\partial \omega}{\partial x_j}\right] \tag{6}$$

Closure coefficient and auxiliary relations used in Eqs. (4), (5) and (6) $\alpha = \frac{5}{9}$, $\beta = \frac{3}{40}$, $\beta^* = \frac{9}{100}$, $\sigma = \frac{1}{2}$, $\sigma^* = \frac{1}{2}$, $\varepsilon = \beta^*\omega k$

Numerical studies using a CFD program, several assumptions are defined to make the problem more plausible and simple. These assumptions can be listed as:

- Flow was constant and turbulent,
- There was no velocity slip on the walls (no slip condition was applied),
- Bidirectional connection was adopted for solid–liquid zones and the effect of radiation heat transfer was ignored,
- The refrigerant air enters through the inlet section with a fully developed velocity profile at 300 K.

4 Boundary conditions

Intel, one of the largest CPU manufacturers in the world, has developed air and liquid-cooled systems. Explained how the cooling system works as follows: The heat generated by the processor itself is distributed to the metal lid of the CPU, called the Integrated Heat Spreader (IHS). The heat is then transferred to the baseplate of the CPU cooler. That heat is then distributed, either by liquid or via heat pipe, to a fan, where it is blown away from the cooler and eventually away from the PC [29]. Therefore, the fins are not placed directly into the CPU, but in the heat sink base in contact with the CPU ceiling plate (IHS). In Fig. 2, this situation and boundary conditions are clearly shown.

All micro-pin–fin channel flow simulations were performed with a computational fluid dynamics (CFD) software, ANSYS-Fluent. As stated in mathematical expression, the k-ω turbulence model was used. Extensive information about turbulence models can be found in the literature. [30–33]. The same type of triangular cell mesh structure was adopted for all study models. The areas close to the boundary walls and fin surfaces were more densely meshed to obtain results accurately and precisely. Furthermore, inflation (20 layer) was used on the fin surfaces where heat transfer is most effective and on the contact surfaces of the fin surface and the heat sink. In the solution settings of the discretization scheme, "Second Order Upwind" were set in momentum and "Coupled" were used in the numerical scheme. For all solid surfaces, the fluid velocity was set to "zero" for the no slip boundary condition and the turbulence intensity was adopted to 0.5%. All solid surfaces of the heat sink were defined to be adiabatic except the bottom surface where the fins are in contact. In the computation, the convergence criterion between two consecutive iterations, which is important

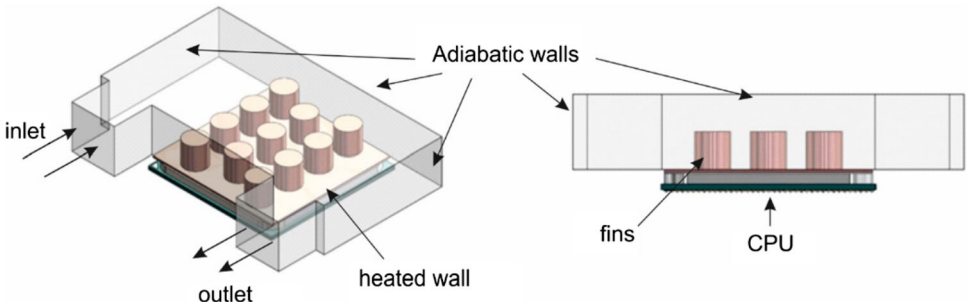

Fig. 2 View of micro-channel (heat sink), and micro-pin–fins placed on the CPU

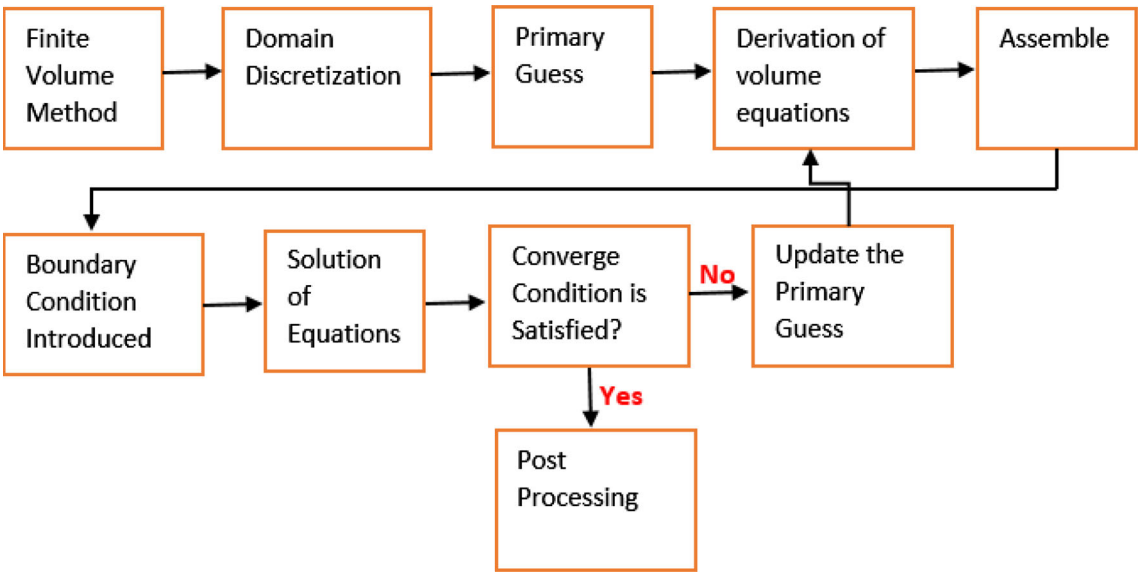

Fig. 3 Outline of finite volume procedure

Table 2 Average Nusselt number and temperature values according to the number of mesh elements

Mesh element	8450	12,825	24,720	53,456	91,832	177,576	236,328	334,128	511,240
Nusselt number	3.339	3.437	3.350	3.480	3.442	3.397	3.375	3.374	3.370
T_{max} (K)	343.02	358.50	345.26	362.15	358.78	349.80	347.95	347.87	347.85

to obtain more precise results, is set as 1×10^{-6} for energy solution and 1×10^{-3} for continuity and momentum solution. Figure 3 demonstrates the outline finite volume procedure used.

In numerical analysis, it is extremely important to achieve mesh independence before proceeding to all analyses. In order to ensure mesh independence, the output parameter is determined and its change is monitored with the change in the number of elements. Nusselt number and maximum temperature value of channel were used as the output parameter in the study and mesh independence analysis was started. The obtained results with the increase of the mesh number are given in Table 2 to understand the variation and to determine the optimal mesh number. The variation of Nusselt numbers and maximum channel temperature for the mesh element of 236,000 above is at appropriate and usable levels. Considering the solution times of the analysis and the computer capacity used, the simulation was started with 250,000 mesh elements. In Fig. 4, the views of the mesh structure used in this study, which were determined after the mesh independence method, are shown in detail for the working models.

By performing the analyzes in a specific Re number [25] range, after processing the analysis results, the average Nusselt number (Nu_{avg}) [11] and the surface friction factor (f) are estimated with the following expressions:

$$\mathrm{Re} = \frac{\rho . V . D_{\mathrm{h}}}{\mu} \tag{7}$$

$$D_h = \frac{4 \cdot A_{\mathrm{in}}}{P_{\mathrm{in}}} \tag{8}$$

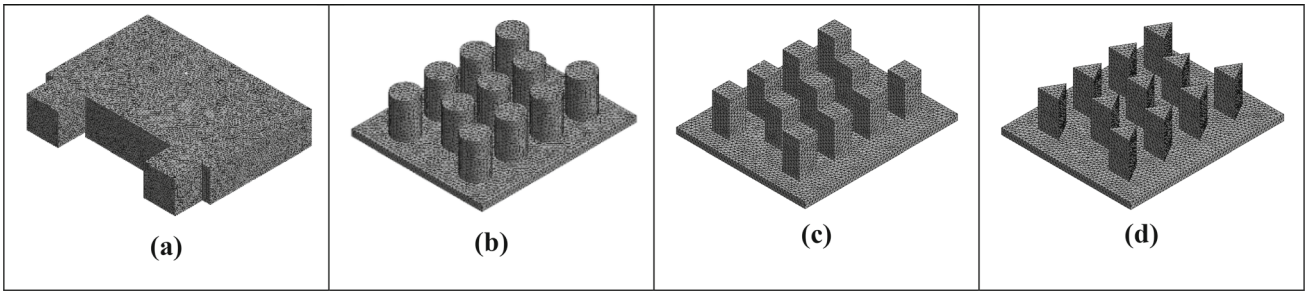

Fig. 4 Microchannel mesh structure view **a** channel **b** circular fins **c** square fins **d** triangular fins

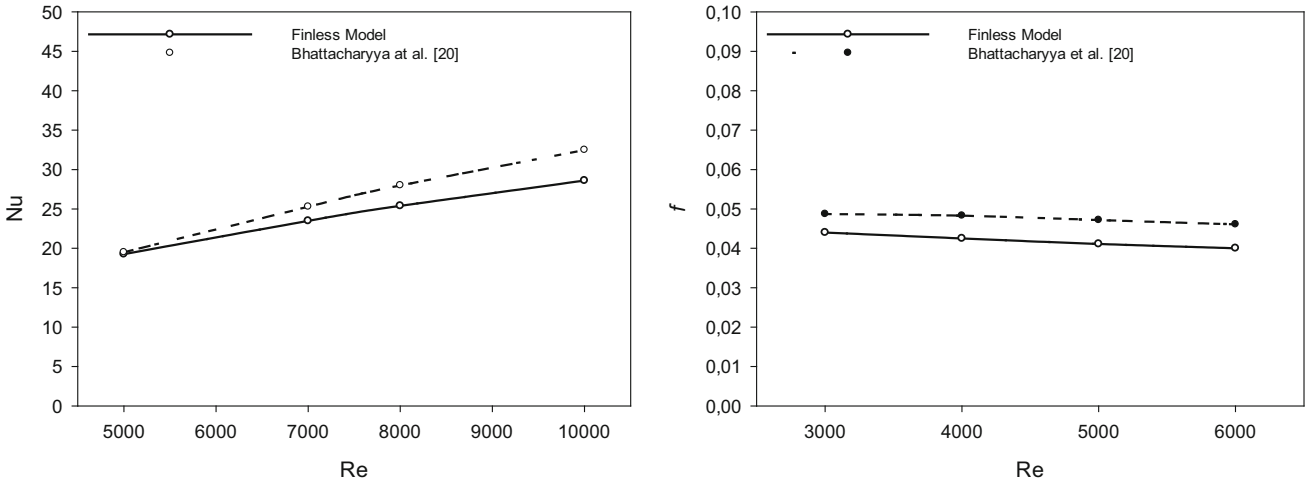

Fig. 5 Comparison with open literature **a** Nu–Re **b** f–Re

In Eq. (7), ρ is the density of the fluid air, V is the fluid velocity, D_{h} is the channel inlet hydraulic diameter, and μ is the fluid viscosity. The hydraulic diameter D_{h} is obtained from the ratio of the inlet cross-section area (A_{in}) and perimeter (P_{in}) as given in Eq. (8).

$$\mathrm{Nu}_{\mathrm{avg}} = \frac{h_{\mathrm{avg}} * S_{\mathrm{fin}}}{k} \tag{9}$$

$$h_{avg} = \frac{h_{\mathrm{fin}} A_{\mathrm{fin}} + h_{\mathrm{b}} A_{\mathrm{b}}}{A_{\mathrm{fin}} + A_{\mathrm{b}}} \tag{10}$$

In Eq. (9), h_{avg} is the average heat transfer coefficients, $\mathrm{S}_{\mathrm{fin}}$ is the surface area of fins, and k is the heat conductivity coefficient. In Eq. (10), A_{b} and A_{fin} represent the total base wetted surface area and fin surface areas, respectively.

$$f = \frac{\Delta P \cdot D_{\mathrm{h}}}{2 \cdot \rho \cdot V^2 \cdot L} \tag{11}$$

Solutions were made between the values of Re = 5000 and Re = 10,000 by using the geometric model and boundary conditions in the reference study for the verification of the presented study and its compatibility with the literature. In Fig. 5, the Nu–Re and f–Re graphs of the study by Bhattacharyya et al. [23] and the presented study are given comparatively. The difference is due to the different turbulence intensity used in the previous study. As expected, this situation increases with the increase of Re number. The important rule in model comparison studies is to keep the boundary conditions constant in the analyses for all models. Therefore, this rule was applied in the study.

5 Results and discussion

In order to analyse the thermal and dynamic performances of the heat sink channel, 4 different models with finless, circular finned, triangular finned and square finned were analysed by taking 28 different solutions between Re = 500 and Re = 10,000 values. Streamlines and temperature contours are given in Fig. 6 for Re = 500, Fig. 7 for Re = 5000, and Fig. 8 for Re = 10,000. The circulation of the flow in the heat sink channel and its direct contact with the fin surfaces are the most important factors affecting the heat transfer. It can be clearly seen from the figures that the use of fins significantly affects this situation.

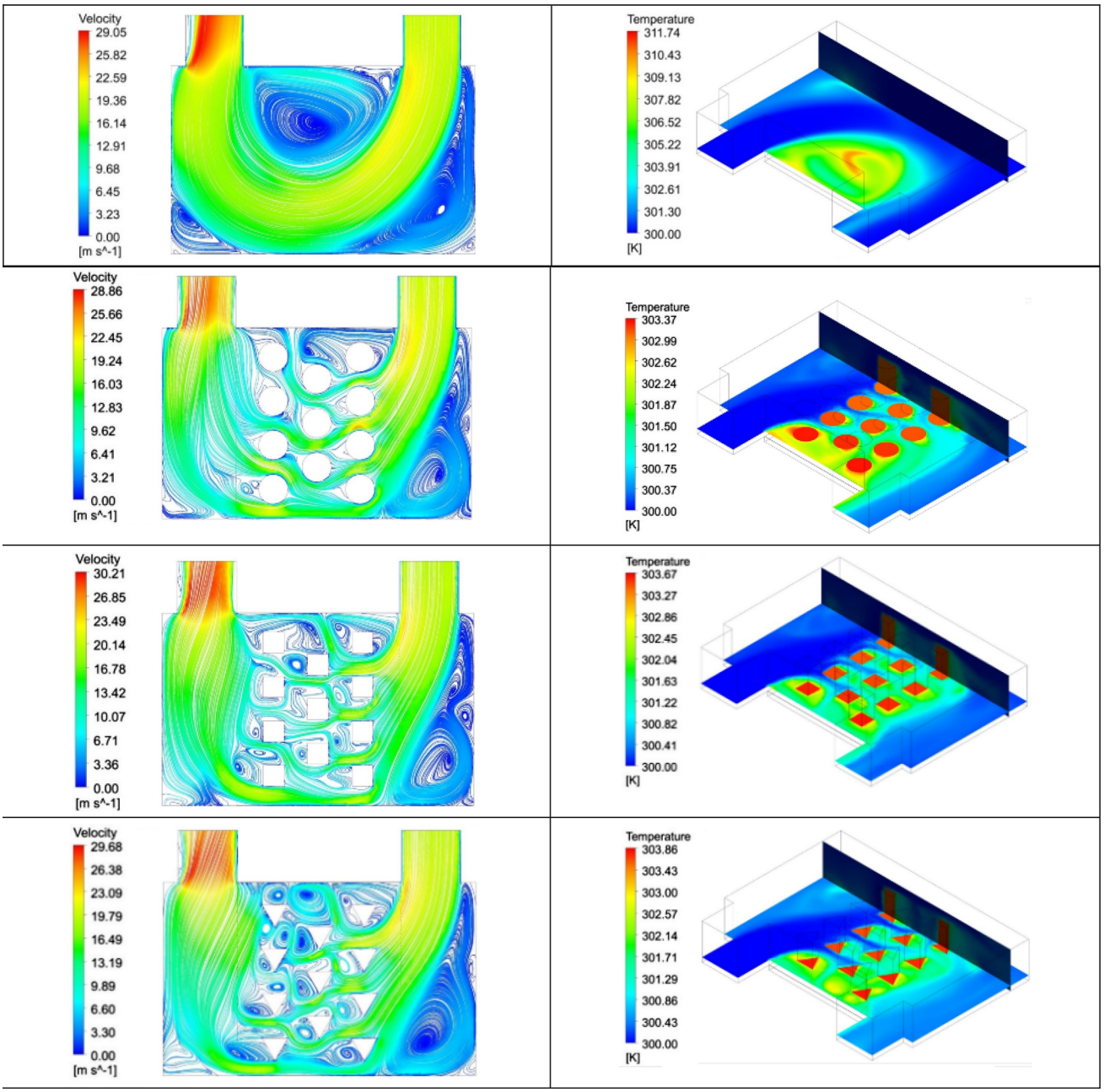

Fig. 6 Streamlines and temperature contours for Re = 500 **a** finless model, **b** circular fin model, **c** square fin model, **d** triangular fin model

In Fig. 6, streamlines and temperature contours of all models at Re = 500 are given. It is seen that the large dead zone formed between the inlet/outlet sections in the finless model in the streamlines disappears when the flow is directed to this area with the use of fins. On the other hand, with the use of circular fins in the temperature contours, a decrease of 9.53% was experienced in the maximum temperature values. It was followed by square fin models with 9.20% and triangular fin models with 8.76%.

In Fig. 7, streamlines and temperature contours of the finless model and the finned models are given at Re = 5000. It has been observed that the fluid reaches the regions between the fins more with the increase of the Reynolds number. Thus, the contact surface has increased and the heat transfer performance has improved. The flow velocity in the eddies formed after the fins also increased. The use of circular fin has reduced the maximum temperature values in the model by 2,68% compared to the finless model. It was followed by square fin models with 2.58% and triangular fin models with 2.53%.

Figure 8 shows the streamlines and temperature contours of all models at Re = 10,000. In the finless model, the dead zone formed between the inlet/outlet sections is distributed more with the fins and its effect on heat transfer is increased by contacting the fin

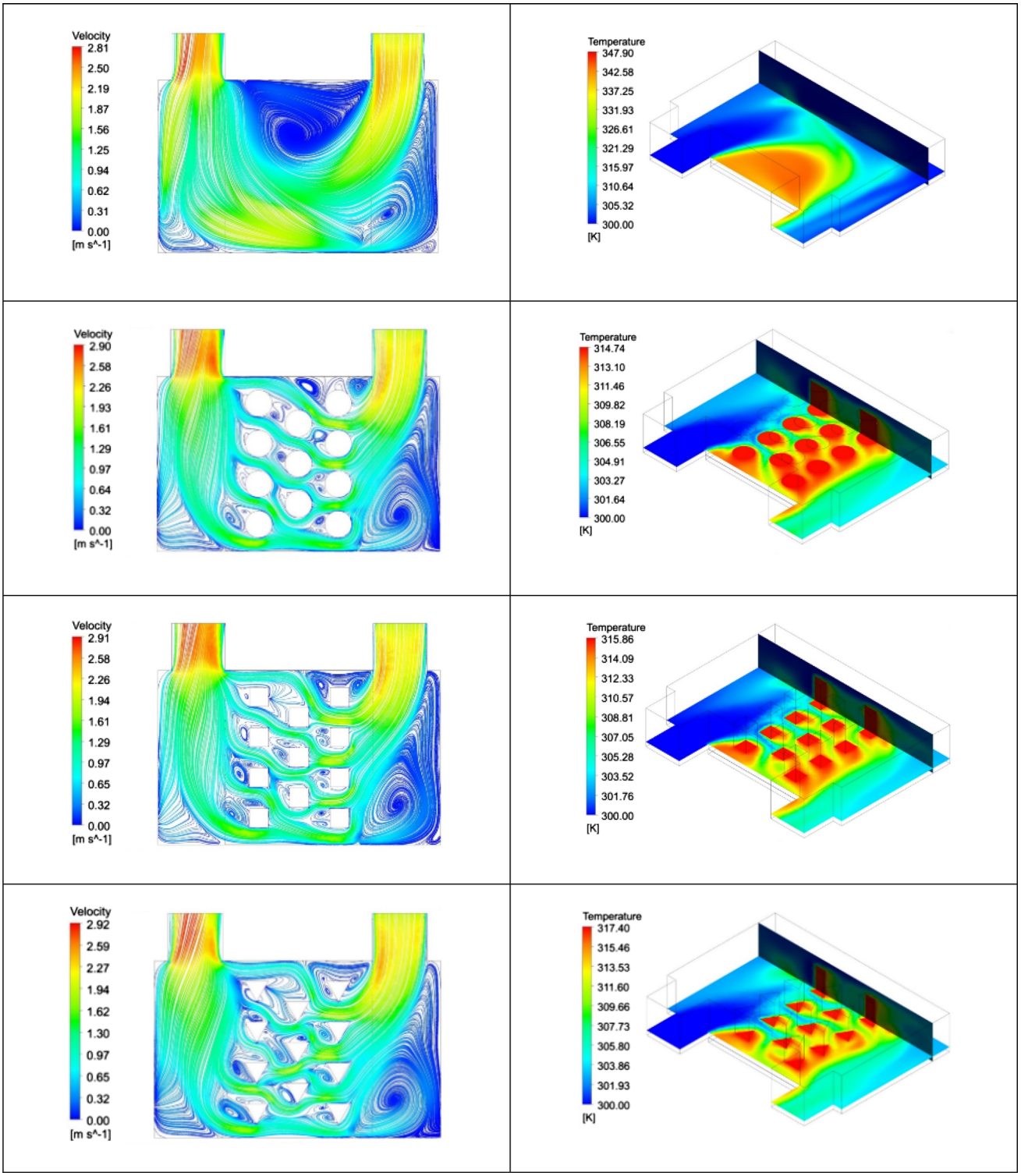

Fig. 7 Streamlines and temperature contours for Re = 5000 **a** finless model, **b** circular fin model, **c** square fin model, **d** triangular fin model

surfaces. The use of circular fin has reduced the maximum temperature by 1,44% at Re = 10,000. It was followed by square fin models with 1.36% and triangular fin models with 1.31%.

It is clearly seen from figures that in-channel circulation is more in the models with fins while the fluid is directed towards the outlet in the finless model. In the axial direction of the inlet, vortices occurred at the corner of the heat sink channel in all models and for each Re number used.

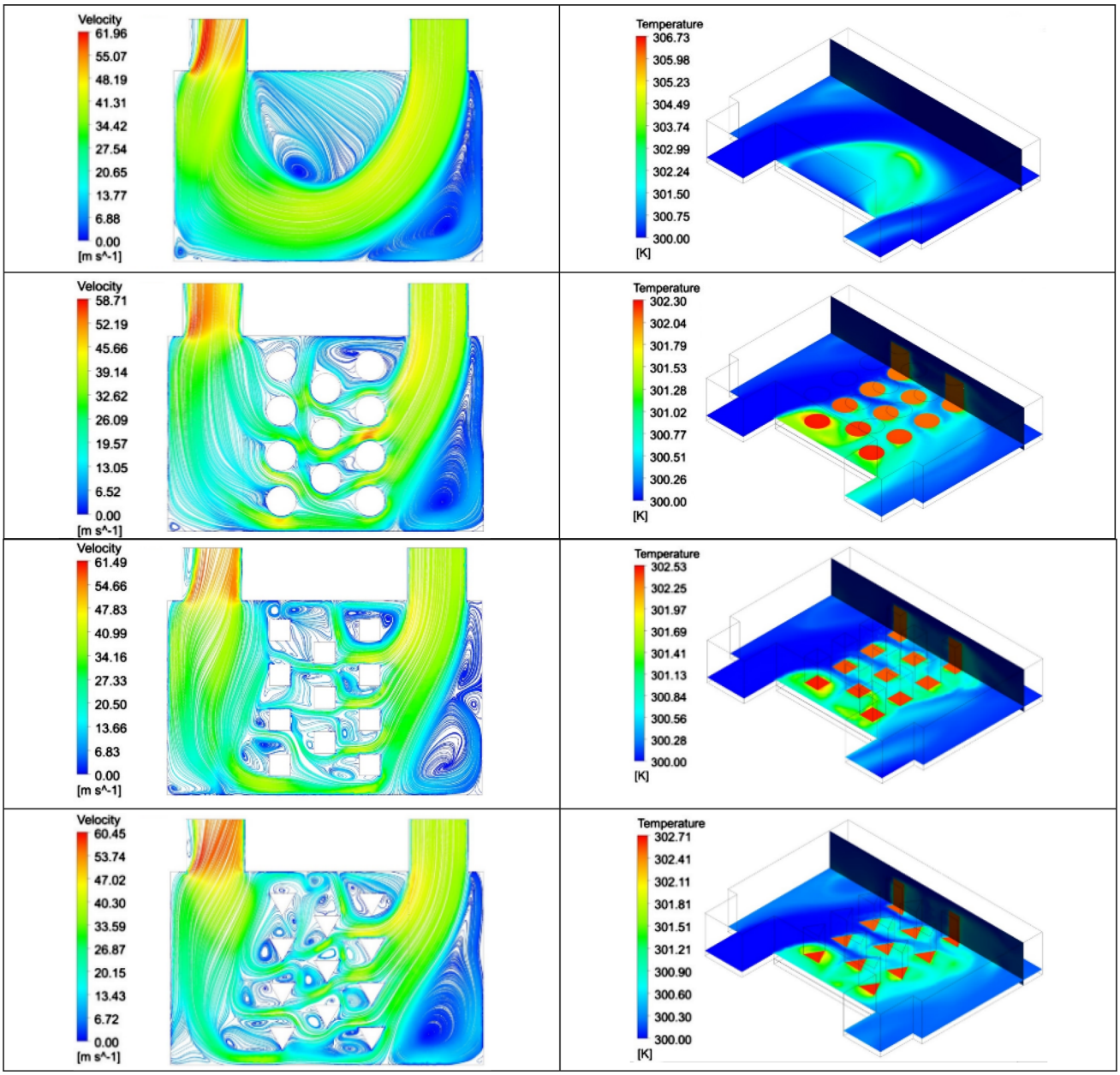

Fig. 8 Streamlines and temperature contours for Re = 10,000 **a** finless model, **b** circular fin model, **c** square fin model, **d** triangular fin model

The temperature contours of all models show that the fluid does not have sufficient cooling effect at all Re numbers in the finless model. The maximum temperature in the model decreased from 347.90 to 314.74 K with the use of circular fins at Re = 500. At the value of Re = 5000, it is seen that the maximum temperature drops from 311.74 to 303.37 K. It is clearly seen that the cooling performance has improved with the use of fins in all remaining temperature contours. The best cooling performance in all Reynolds number values was obtained in the circular fin model. The circular fin model was followed by the square fin model and the triangular fin model, respectively.

In order to understand how the heat transfer over the heated base surface plate of the heat sink changes across the surface, "lines" were assigned between the fins as seen in Fig. 9. Line 1 was positioned vertically in the middle of the inlet and outlet sections, and Line 2 was positioned horizontally at the plate length in the middle of the channel. The temperature changes along Line 1 and Line 2 were obtained at the dimensionless x/L distance.

Figure 10.a shows the temperature change graphs on Line 1 for Re = 500, 5000 and 10,000 values. The highest temperature values along Line 1 is seen in the finless model at all Reynolds numbers. A sudden temperature drop is seen at the point where the x/L length is 0.1, which is dimensionalized depending on the channel length of the finless model. This drop is due to the fact that the fluid passes through the flow area by drawing only a U between the inlet and outlet sections, since there is no fin. Fluctuations

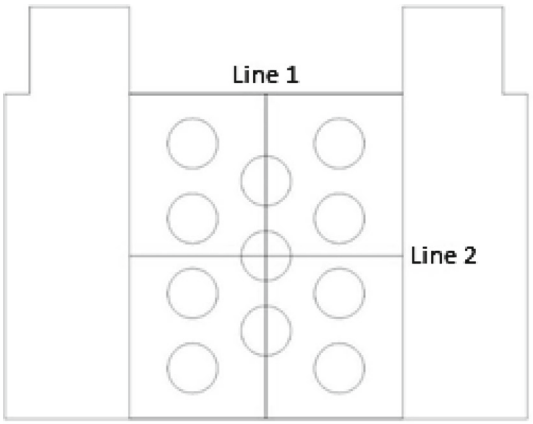

Fig. 9 View of the Line 1 and Line 2 locations

have been occurred on the temperature graphs of the models using fins. The points where the temperature increases are the places where the fins are located. The fins are in a heated state due to heat exchange with the heated plate. In the finless model, the fin temperature, which was 347.07 K at x/L 0.78 at Re = 500 value, decreased to 301.79 K at the same point at Re = 10,000. In the circular fin model, the temperature at x/L 0.78 was 314.58 K at Re = 500 and 302.22 K at Re = 10,000. This temperature decreased from 315.70 K to 302.46 K in the square fin model and from 317.18 K to 301.91 K in the triangular fin model.

In Fig. 10.b, temperature graphs on Line 2 are given for Re = 500, 5000 and 10,000 values. The highest temperature values along Line 2 is seen in the finless model, as in Line 1. In models with circle fins and square fins, there is only 1 fin between points 0.45 and 0.65 along Line 2. While the maximum temperature values are reached at this point for the circle and square fin models, the triangular fins model remains at low temperatures at these points due to the geometric layout. Sudden temperature changes in the finless model are directly related to the path followed by the fluid. In the finless model, the temperature which was 344.40 K at x/L = 0.78 at Re = 500, decreased to 304.06 K at the same point at Re = 10,000. In the circular fin model, the temperature was 314.14 K at x/L = 0.78 at Re = 500 and 300.65 K at Re = 10,000. This temperature has been reduced from 315.08 K to 301.6 K in the square fin model and from 316.59 K to 301.07 K in the triangular fin model.

In Fig. 11, the effects of Reynolds (Re) number on pressure drop, average Nu number, average skin friction value and PEC number are given. These parameters were studied in the Re number range of 500 to 10,000. The effect of Re number on pressure drop is presented in Fig. 11a. Accordingly, with the increase of Re number, the pressure drop increases in all models. The lowest pressure drop is observed in the finless model, while the highest values are observed in the square finned model. It is followed by the triangular fin model and the circular fin model, respectively. It can easily be said that the circular fin model is superior to other finned models in terms of pressure drop. Furthermore, with the increase of Re number, the inlet–outlet section pressure drop range between the models increased. While the pressure drop in the square finned model is 1100 Pa in Re = 10,000, this value was obtained in the triangular fin model 1000 Pa at same Re, in the circular fin model 650 Pa and in finless model 600 Pa.

Figure 11b shows the change in the mean Nusselt number with increasing Reynolds number. The Nusselt number indicates the heat transfer improvement as a result of the convection to conduction ratio over a fluid layer. A large Nusselt number indicates that convection is more effective. In Fig. 11b, Nu numbers increase with increasing Re numbers. A significant difference was observed in all fin models compared to the finless model. This difference between the Nusselt numbers clearly shows the importance of the use of fins. When the numerical values are examined at Re = 10,000, the highest Re number, while the Nu number in the finless model was obtained as 20, in the triangular model as 37, in the square model as 40 and in the circular model as 43.

Figure 11c gives the average skin friction variation with Reynolds number. Friction values decrease with Re number in all models. Friction values are the lowest as would be expected for the finless model without any pin–fin barrier. It has been followed by models with circular fins, triangular fines and square fins, respectively. It can be said that this order is directly related to the aerodynamic structures of the fins. The friction factor of the circular fin model has been observed 28.62% less than the square fin model and 25% less than the triangular fin model at Re = 5000. In Re = 10,000, it has been found that the results were 33.94 and 29.49% lower than the square and triangular fin models, respectively.

The thermal performance factor is a function of the Nusselt number and the friction factor and is called the PEC (Performance Evaluation Criteria) number. The PEC number is a measure of how effectively heat transfer is increased despite hydrodynamic forces [34]. Therefore, it is important to explain how efficient a cooling surface is by using PEC number. Higher PEC values obtained from the system indicate that it provides higher heat transfer. Also, the obtained PEC value greater than 1 indicates that the heat transfer rate is greater than the increase in pressure drop [35, 36]. PEC number is obtained by the Eq. 12:

$$\mathrm{PEC} = \frac{\mathrm{Nu}/\mathrm{Nu_o}}{\mathrm{f}/\mathrm{f_o}^{(1/3)}} \tag{12}$$

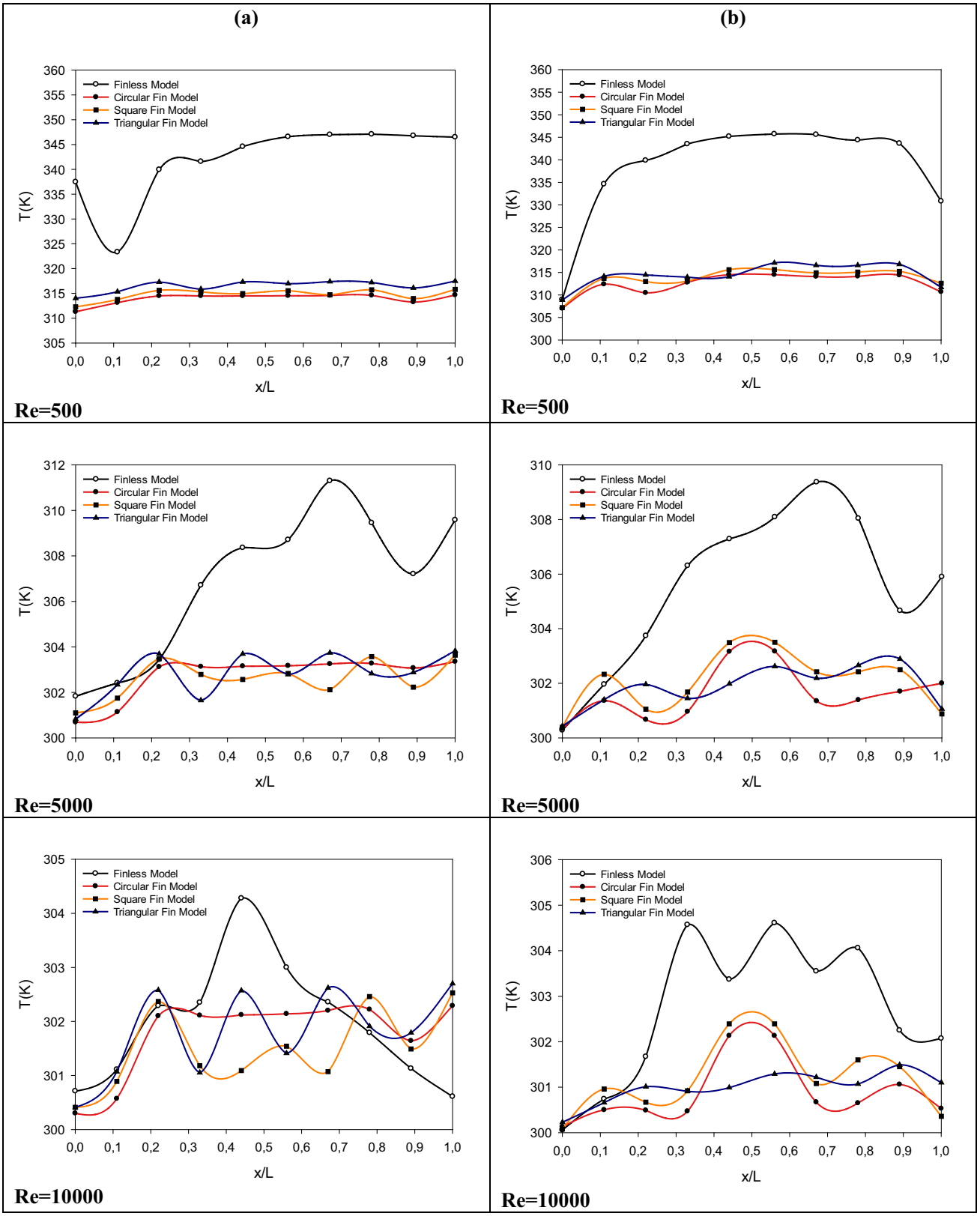

Fig. 10 Temperature changes on **a** Line 1 and, **b** Line 2 at different Re numbers

Here; Nu is the mean Nusselt number for the model with fins, Nuo is the Nusselt number for finless model, f is the average surface friction coefficient for the finned model, and fo is the mean surface friction coefficient for the finless model.

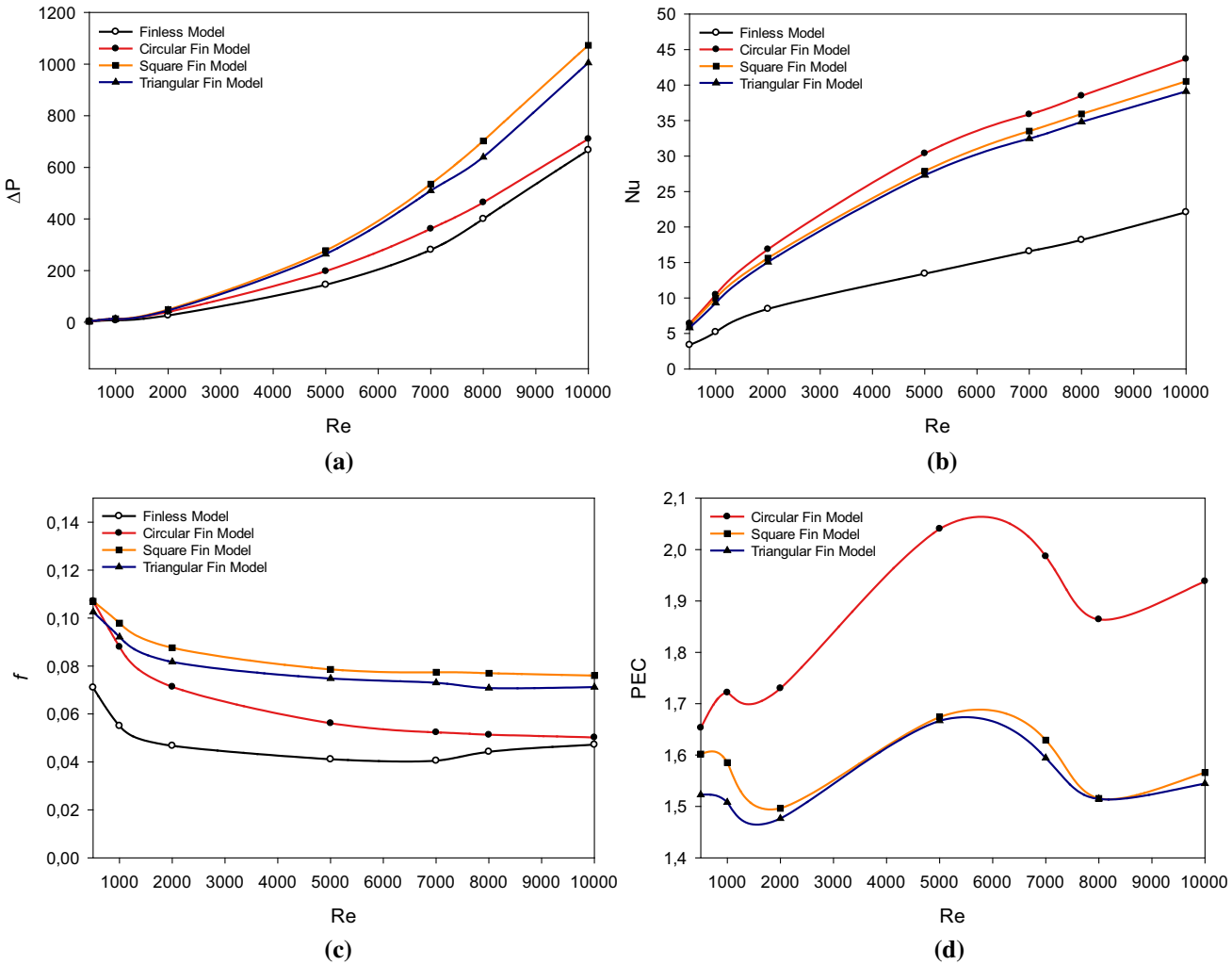

Fig. 11 Effect of Reynolds (Re) numbers on **a** pressure drop (ΔP), **b** Nusselt number (Nu), **c** skin friction (f) and **d** PEC values

The effect of models with different fin structures on PEC is shown in Fig. 11d for different Re numbers. It can be easily seen from the graph that the most effective operating range is Re 5000–6500. The largest PEC values have been obtained at these points. The best PEC results were obtained in the circular fin model. The PEC number of the circular fin model with Re = 5000 value was 17.96% and 18.30% higher than the PEC numbers of the square fin and triangular fin models, respectively.

6 Conclusion

In this study, the effect of different fin structures on the hydrodynamic and thermal performances of MPFs (micro-pin fin) used for motherboard processor cooling was investigated. The MPF affected the flow circulation over the existing cross-sectional areas and thus the amount of heat transfer over the MPFs. The findings obtained at the end of the study can be listed as follows:

- Re number is one of the important flow parameter in heat sink performance. An increase in the Nusselt number occurred in each geometry with an increase in the Reynolds number. The circular fin model was the model that gave the best results in terms of Nusselt number. The circular fin model was followed by the square fin and triangular fin models, respectively. In addition, the difference between Nusselt values obtained in finless geometry and Nusselt numbers of geometries with fins clearly revealed the importance of using fins.
- Pressure drop has occurred on all models as the Re number increases. These pressure drops are highest in the square fin model. The pressure drop generated in the square fin model at Re = 5000 value is 4.79, 28.67 and 47.7% higher than the models with triangular fins, circular fins and finless, respectively. In all Re numbers, the best results among the fin models in terms of pressure drop has been obtained in the circular fin model.

- The average friction factor, which is accepted as one of the factors causing the pressure drop, decreases with the Re number and as predicted, the lowest values are obtained for the finless model. The finless model with the lowest friction factor has been followed by circular finned, triangular finned and square finned models, respectively. The f values of the circular fin model were 28.62% less than the square fin model and 25% less than the triangular fin model at Re = 5000.
- Performance criterion (PEC) values, which are the most important indicators of the effectiveness of the models, were calculated, and it was determined that the best working range of all models was between Re = 5000 and Re = 6500. The PEC number of the circular fin model at Re = 5000 value was 17.96 and 18.30% higher than the PEC numbers of the square fin and triangular fin models, respectively. The best PEC results were obtained in the circular fin model.
- As a result, in 28 different solutions made at 7 different Reynolds numbers for 4 different models, the heat transfer over the circular fin model was found to be the most effective in the range Re = 5000–6500, and it was concluded that it could be used in this range compared to other models.
- As in the heat sink systems used in the current study, which is determined as optimum fin, can be used in several technological and engineering applications like heat exchangers, solar collectors, radiators, gas turbines, air-cooled engines, transformers, electric devices ETC.

The investigation can further be extended to include any novel shape of fins, and fluid or nanofluid can be replaced by air to observe the outcomes.

Acknowledgements I would like to express my special thanks to my colleague Dr. Dogan Engin Alnak who worked with me in this research.

Data Availability Statement This manuscript has associated data in a data repository. [Authors' comment: All dates contained in this manuscript are available upon request by contacting with the corresponding author].

References

1. O. Bayer, Determination of forced convection correlation over finned surfaces in turbulent, fully developed internal flow: parametric experimental analysis. Uludağ Univ J. Fac. Eng. **23**(1), 417–430 (2018). https://doi.org/10.17482/uumfd.376556
2. P. Naphon, S. Wiriyasart, S. Wongwises, Thermal cooling enhancement techniques for electronic components. Int. Commun. Heat Mass Transf. **61**, 140–145 (2015). https://doi.org/10.1016/j.icheatmasstransfer.2014.12.005
3. S.A. Jajja, W. Ali, H.M. Ali, A.M. Ali, Water cooled minichannel heat sinks for microprocessor cooling: effect of fin spacing. Appl. Therm. Eng. **64**(1–2), 76–82 (2014). https://doi.org/10.1016/j.applthermaleng.2013.12.007
4. Y. Wang, B. Wang, K. Zhu, H. Li, W. He, S. Liu, Energy saving potential of using heat pipes for CPU cooling. Appl. Therm. Eng. **143**, 630–638 (2018). https://doi.org/10.1016/j.applthermaleng.2018.07.132
5. I. Mjallal, H. Farhat, M. Hammoud, S. Ali, I. Assi, improving the cooling efficiency of heat sinks through the use of different types of phase change materials. Technologies **6**(1), 5 (2018). https://doi.org/10.3390/technologies6010005
6. G.V. Kewalramani, A. Agrawal, S.K. Saha, Modeling of microchannel heat sinks for electronic cooling applications using volume averaging approach. Int. J. Heat Mass Transf. **115**(111), 395–409 (2017). https://doi.org/10.1016/j.ijheatmasstransfer.2017.08.041
7. M.W. Alam, S. Bhattacharyya, B. Souayeh, K. Dey, F. Hammami, M. Rahimi-Gorji, R. Biswas, CPU heat sink cooling by triangular shape micro-pin-fin: Numerical study. Int. Commun. Heat Mass Transfer **112**, 104455 (2020). https://doi.org/10.1016/j.icheatmasstransfer.2019.104455
8. H.C. Chiu, R.H. Hsieh, K. Wang, J.H. Jang, C.R. Yu, The heat transfer characteristics of liquid cooling heat sink with micro pin fins. Int. Commun. Heat Mass Transf. **86**, 174–180 (2017). https://doi.org/10.1016/j.icheatmasstransfer.2017.05.027
9. D.D. Ma, G.D. Xia, L.X. Zong, Y.T. Jia, Y.X. Tang, R.P. Zhi, Experimental investigation of flow boiling heat transfer performance in zigzag microchannel heat sink for electronic cooling devices. Int. J. Therm. Sci. **145**, 106003 (2019). https://doi.org/10.1016/j.ijthermalsci.2019.106003
10. G.V. Kewalramani, G. Hedau, S.K. Saha, A. Agrawal, Study of laminar single phase frictional factor and Nusselt number in In-line micro pin-fin heat sink for electronic cooling applications. Int. J. Heat Mass Transf. **138**, 796–808 (2019). https://doi.org/10.1016/j.ijheatmasstransfer.2019.04.118
11. J.F. Tullius, T.K. Tullius, Y. Bayazitoglu, Optimization of short micro pin fins in minichannels. Int. J. Heat Mass Transf. **55**(15–16), 3921–3932 (2012). https://doi.org/10.1016/j.ijheatmasstransfer.2012.03.022
12. Y.K. Prajapati, Influence of fin height on heat transfer and fluid flow characteristics of rectangular microchannel heat sink. Int. J. Heat Mass Transf. **137**, 1041–1052 (2019). https://doi.org/10.1016/j.ijheatmasstransfer.2019.04.012
13. H. Chiu, R. Hsieh, K. Wang, J. Jang, C. Yu, The heat transfer characteristics of liquid cooling heat sink with micro pin fins. Int. Commun. Heat Mass Transf. **86**(June), 174–180 (2017). https://doi.org/10.1016/j.icheatmasstransfer.2017.05.027
14. F. Koca, M. Zabun, The effect of outlet location on heat transfer performance in micro pin-fin cooling used for a CPU. Eur. Phys. J. Plus **136**, 1115 (2021). https://doi.org/10.1140/epjp/s13360-021-02113-4
15. H. Abbasi, S. Turki, S.B. Nasrallah, Numerical investigation of forced convection in a plane channel with a built-in triangular prism. Int. J. Therm. Sci. **40**, 649–658 (2001). https://doi.org/10.1016/S1290-0729(01)01254-6
16. J.P. Abraham, E.M. Sparrow, J.C.K. Tong, Heat transfer in all pipe flow regimes: laminar, transitional/intermittent, and turbulent. Int. J. Heat Mass Transf. **52**, 557–563 (2009). https://doi.org/10.1016/j.ijheatmasstransfer.2008.07.009
17. M. Abuşka, S. Şevik, V. Altıntaş, The effect of blowing direction on heat sink performance by thermal imaging. J. Therm. Eng. **4**(6), 2471–2480 (2018). https://doi.org/10.18186/thermal.465695
18. T. Ambreen, M.H. Kim, Flow and heat transfer characteristics over a square cylinder with corner modifications. Int. J. Heat Mass Transf. **117**, 50–57 (2018). https://doi.org/10.1016/j.ijheatmasstransfer.2017.09.132
19. H. Arya, M.M. Sarafraz, M. Arjomandi, Heat transfer and fluid flow of MgO/ethylene glycol in a corrugated heat exchanger. J. Mech. Sci. Technol. **32**(8), 3975–3982 (2018). https://doi.org/10.1007/s12206-018-0748-x
20. N. Acharya, Buoyancy driven magnetohydrodynamic hybrid nanofluid flow within a circular enclosure fitted with fins. Int. Commun. Heat Mass Transf. **133**, 105980 (2022). https://doi.org/10.1016/j.icheatmasstransfer.2022.105980
21. N. Acharya, A.J. Chamkha, On the magnetohydrodynamic Al2O3-water nanofluid flow through parallel fins enclosed inside a partially heated hexagonal cavity. Int. Commun. Heat Mass Transf. **132**, 105885 (2022). https://doi.org/10.1016/j.icheatmasstransfer.2022.105885

22. N. Acharya, On the hydrothermal behavior and entropy analysis of buoyancy driven magnetohydrodynamic hybrid nanofluid flow within an octagonal enclosure fitted with fins: application to thermal energy storage. J. Energy Storage **53**, 105198 (2022). https://doi.org/10.1016/j.est.2022.105198
23. S. Bhattacharyya, B. Souayeh, A. Banerjee, R. Sarkar, Numerical analysis of micro-pin-fin heat sink cooling in the mainboard chip of a CPU. Eur. Phys. J. Plus **123**, 1–10 (2020). https://doi.org/10.1140/epjp/s13360-020-00359-y
24. N. Sahiti, A. Lemouedda, D. Stojkovic, F. Durst, E. Franz, Performance comparison of pin fin in-duct flow arrays with various pin cross-sections. Appl. Therm. Eng. **26**(11–12), 1176–1192 (2006). https://doi.org/10.1016/j.applthermaleng.2005.10.042
25. H.R. Seyf, M. Feizbakhshi, Computational analysis of nanofluid effects on convective heat transfer enhancement of micro-pin-fin heat sinks. Int. J. Therm. Sci. **58**, 168–179 (2012). https://doi.org/10.1016/j.ijthermalsci.2012.02.018
26. L. Gong, J. Zhao, S. Huang, Numerical study on layout of micro-channel heat sink for thermal management of electronic devices. Appl. Therm. Eng. **88**, 480–490 (2015). https://doi.org/10.1016/j.applthermaleng.2014.09.048
27. X. Han, S. Krajnović, Very-large-eddy simulation based on k-ω model. AIAA J. **53**(4), 1103–1108 (2015). https://doi.org/10.2514/1.J053341
28. C. David, Wilcox, Reassessment of the scale-determining equation for advanced turbulence models. AIAA J. **26**(11), 1299–1310 (1988). https://doi.org/10.2514/3.10041
29. url: https://www.intel.com/content/www/us/en/gaming/resources/cpu-cooler-liquid-cooling-vs-air-cooling.html
30. M.M. Doustdar, H. Alipour, M. Aliakbari, Estimating spray characteristics of the air-blast atomizer of a typical jet engine using definition of the new non-dimensional number K: numerical and experimental study. Tehnički vjesnik **29**(1), 208–214 (2022). https://doi.org/10.17559/TV-20200813084024
31. K. Khani Aminjan, M. Heidari, D.D. Ganji, M. Aliakbari, F. Salehi, M. Ghodrat, Study of pressure-swirl atomizer with spiral path at design point and outside of design point. Phys. Fluids **33**(9), 093305 (2021). https://doi.org/10.1063/5.0059779
32. K. Khani Aminjan, M. Heidari, P. Rahmanivahid, Study of spiral path angle in pressure-swirl atomizer with spiral path. Arch. Appl. Mech. **91**(1), 33–46 (2021)
33. A. N. S. Y. S. Fluent, ANSYS Fluent 12.0 user's guide. Ansys Inc, 15317, 1–2498 (2009)
34. T.T. Goksu, I.H. Yılmaz, Enhancement of heat transfer using twisted tape insert in a plain tube. BEÜ Fen Bilimleri Dergisi BEU **8**(1), 251–260 (2019). https://doi.org/10.17798/bitlisfen.462169
35. O. Manca, S. Nardini, D. Ricci, A numerical study of nano fluid forced convection in ribbed channels. Appl. Therm. Eng. **37**, 280–292 (2012). https://doi.org/10.1016/j.applthermaleng.2011.11.030
36. C. Chang, P. Xiaodong, N. Binjian, Heat transfer enhancement of a molten salt parabolic trough solar receiver with concentric and eccentric pipe inserts. Energy Procedia **142**, 624–629 (2017). https://doi.org/10.1016/j.egypro.2017.12.103